Particle deformation and sliding during compaction of spherical powders: a study by quantitative metallography

H. F. Fischmeister, E. Arzt, and L. R. Olsson

The development of contact facets between particles during compaction of a spherical bronze powder is studied in isostatic and uniaxial compression. Non-radial particle motion (particle sliding or 'restacking') is revealed by the eccentricity of the contact flat with respect to the initial point of contact, the latter being marked by a neck formed during light presintering of the powder bed. (The presintering does not seriously affect subsequent compaction.) From these observations, it is concluded that particle sliding occurs up to a pressure at which the original porosity has been about halved. The number of contacts per particle changes gradually from 7·3 in the uncompacted powder to about 12 at 2·5% residual porosity. At the end of densification, the contact number changes very quickly and the particle shape at full density can be approximated by a tetrakaidekahedron. The measurements of coordination number and contact flattening suggest that isostatic ompaction involves less sliding and more deformation of the particles than occurs in uniaxial compression.

Serial No. 477. Manuscript received 14 August 1978. H. F. Fischmeister, Dr phil, is in the Department of Engineering Metals, Chalmers University, Gothenburg, Sweden, and the Department of Physical Metallurgy and Materials Testing, Montanuniversität Leoben, Austria. Mr E. Arzt is in the same department at Leoben, and tekn dr L. Olsson in the same department at Gothenburg.

The compaction of spherical particles, and especially the development of flat contacts between them, is attracting increasing interest in connection with the technical use of gas-atomized powders. For instance, one of the routes suggested for the processing of tool-steel powders incorporates a cold-isostatic precompaction step designed to enlarge the contact surface between the particles in order to improve the heat conductivity of the powder mass before hot-isostatic pressing.[1] Another important aspect of the contact geometry of plastically deformed particles lies in its effect on the kinetics of sintering, which has been demonstrated very clearly by Wellner *et al.*[2] Finally, the increase of particle contact area raises the resistance of a particle system to further compaction. This geometrical strain hardening has an important influence on the pressure/density relationship during compaction. Sundström and Fischmeister[3] have demonstrated that in the porosity range of technical compacts, the increase in contact area is, in fact, more important for the stress required to promote densification than the strain hardening of the particle material itself.

Precise information about the progress of contact flattening during compaction is required to develop a better understanding of the compaction process. James[4–6] has reported measurements of contact flattening for several types of powders by evaluation of scanning electron micrographs of fractured compacts. In the present study, quantitative metallography is combined with scanning electron microscopy (SEM) in the stereo mode to obtain more detailed and reliable information. Quantitative metallography allows the total contact area in a compact to be determined in a straightforward manner from polished sections, irrespective of the shape of particles or contact faces, and without the risk of bias inherent in the evaluation of fracture surfaces.

Many authors have suggested that the compaction of powders should be considered as a multi-stage process. The development of these concepts has been reviewed by Bockstiegel and Hewing,[7] and by James.[8] Several authors suggest a first stage of 'transitional restacking' without plastic deformation.[9,10] The densification associated with this stage is of the order of a few per cent for ductile powders of relatively smooth shape;[9,11–14] with irregular particle shape, and for powders which are difficult to deform, the restacking effect may be much larger.[15,16]

One would expect this stage to be followed by one in which plastic deformation proceeds simultaneously with a diminishing amount of sliding (or non-radial particle motion) until friction, plastic deformation, and cold welding lock the particles into a rigid arrangement in which only plastic deformation can bring about further densification. As pointed out by James[8] and others,[17] there is little experimental evidence concerning this second stage. However, particle sliding is often invoked to explain observed peculiarities of pressure vs. density and of pressure vs. green strength relations.[5,9,10,14,18]

The assessment of non-radial particle motion under pressure—at least in a semi-quantitative manner—forms the second objective of the present study. In experiments on the compaction of presintered powders, it had been observed that the initial points of contact were clearly marked on fracture surfaces by the necks formed during sintering. It was further noticed that the contours of the final

SYMBOLS

Z	Average coordination number
Π	Porosity or volume fraction of pores
V_V^p	Volume of pores per unit volume of specimen
P_t	Total number of points investigated
P_P^p	Fraction of points falling in the pore space (index p)
S_V	Total surface area in unit volume of specimen
P_L	Number of intersections between surface and test line per unit length of test line
P_L^{mm}	Number of intersections with metal–metal contact surface per unit length of test line
P_L^{mp}	Number of intersections with metal–pore contact surface per unit length of test line
R	Volume-weighted mean particle radius
A	Average contact area
C_m	Contiguity of the metal phase
S_V^{mm}	Absolute area of metal–metal contact per unit volume of specimen
$S_{V_m}^{mm}$	Absolute area of metal–metal contact per unit volume of particle phase
V	Mean particle volume $= 4\pi R^3/3$
L	Particle edge length
d	Face diagonal

contact surfaces were often eccentric to the initial contact points. This eccentricity could be evaluated to assess the occurrence of particle sliding; the compaction of the bronze powder used in this study was not seriously disturbed by the light presintering necessary to mark the initial contact points.

EXPERIMENTAL

Gas-atomized spherical bronze powder of composition Cu–11%Sn–0·5%P was used. This powder is normally employed for the fabrication of sintered filters. Its particle size ranged from 100 to 350 μm. A size fraction between 250 and 315 μm was separated by sieving. This had the size distribution shown in Fig. 1; its tap density was 5·47 Mg m^{-3}, corresponding to a porosity of 37·5%. The as-received powder had a heavily segregated solidification structure with interdendritic δ-phase which made the particles somewhat brittle. Therefore, it was annealed in hydrogen for 40 min at 700°C, which produced structural homogeneity and reduced the hardness to a level of about 160 units (μDPI) that remained unchanged by further annealing.

The annealed powder was compacted in a cylindrical, floating die of 25 mm diameter to give compacts of about 15 mm in height. No lubricant was used. To test the compaction behaviour of powder whose particles were bonded to each other by sintered necks, loose powder was filled in a cylindrical stainless steel mould whose diameter was slightly smaller than that of the compaction die, and sintered at 700°C in hydrogen for either 1 or 18 h. Sintering of the particles to the mould was prevented by slight oxidation of the latter. The sintered compacts were compacted in the die in the same way as the unsintered powder. The average diameter of the sintered necks in the compacts prior to pressing was 6·6% of the particle diameter after 1 h and 12% after 18 h sintering.

The compaction curves are shown in Fig. 2. Counter to expectation, the bonded powders were found to densify a little more easily than the unsintered material. The difference between the three curves in Fig. 2 lies mainly in

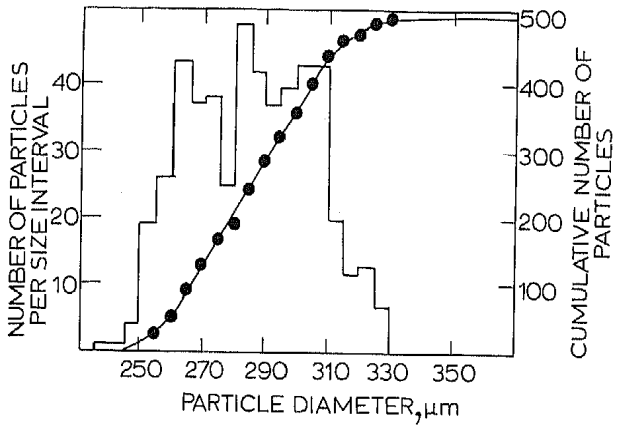

1 Size distribution of particles.

the starting density and in the initial densification up to 0·2 GN m^{-2}; thereafter, the curves can be brought to almost perfect coincidence by appropriate upward shifts. Microhardness measurements showed that the faster densification of the presintered specimens was not caused by softening of the material during sintering. The difference in initial compaction behaviour is attributed to the fact that the presintered compacts fit loosely in the die, and that particle motion in them is restricted. Both points would delay the development of strong friction between powder and die wall which impedes densification in the centre of the compact. It is known from the field of powder forging that coherent powder billets show very little lateral expansion in the early stages of upsetting.[19,20]

MEASUREMENT OF NUMBER OF CONTACTS

The number of neighbours in contact with a particle, or its coordination number, is an important parameter of particle packings. It may be determined from the SEM stereo fractographs on the assumption that, on average, exactly one-half of the contact facets can be seen, the other half being situated on the hidden side of the particles. Between 30 and 75 particles were evaluated for each fracture surface.

The importance of avoiding bias made it desirable to find a more direct method. Several approaches were tried until the following procedure was adopted: a fragment from the central part of the specimen was immersed in Wallner's etching solution[21] ($FeCl_3$, $(NH_4)_2S_2O_8$, and HCl in water)

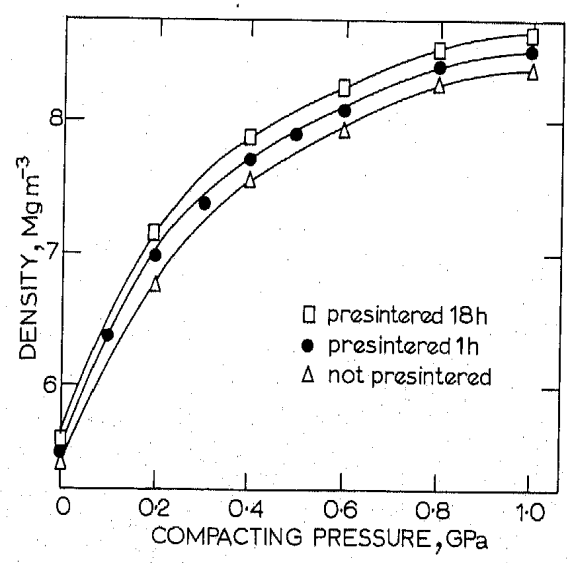

2 Compaction curves (uniaxial compression).

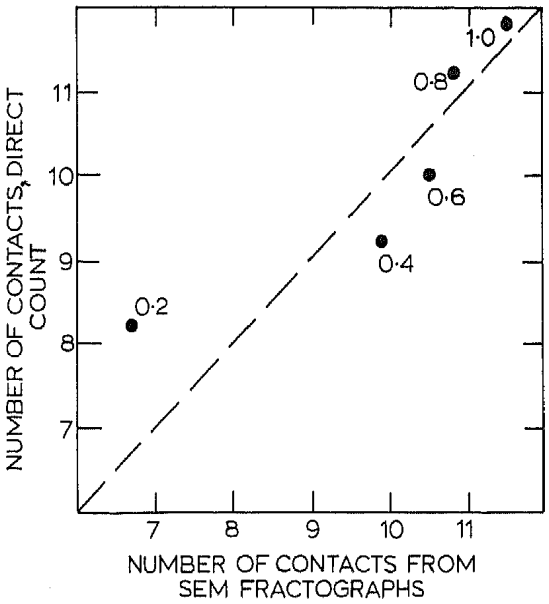

3 Average number of contacts per particle: direct counting results compared to evaluation of SEM fractographs. Parameter: pressure in GN m^{-2}.

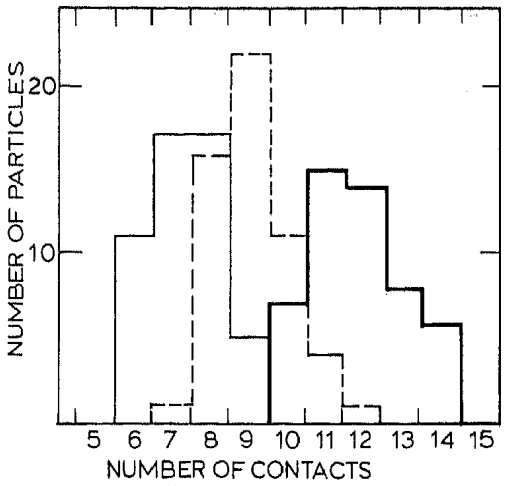

4 Number of particles having given number of contacts: uncompacted (————), compacted at 0·2 GNm^{-2} (——) and at 1 GNm^{-2} (————). Method of measurement: direct counting.

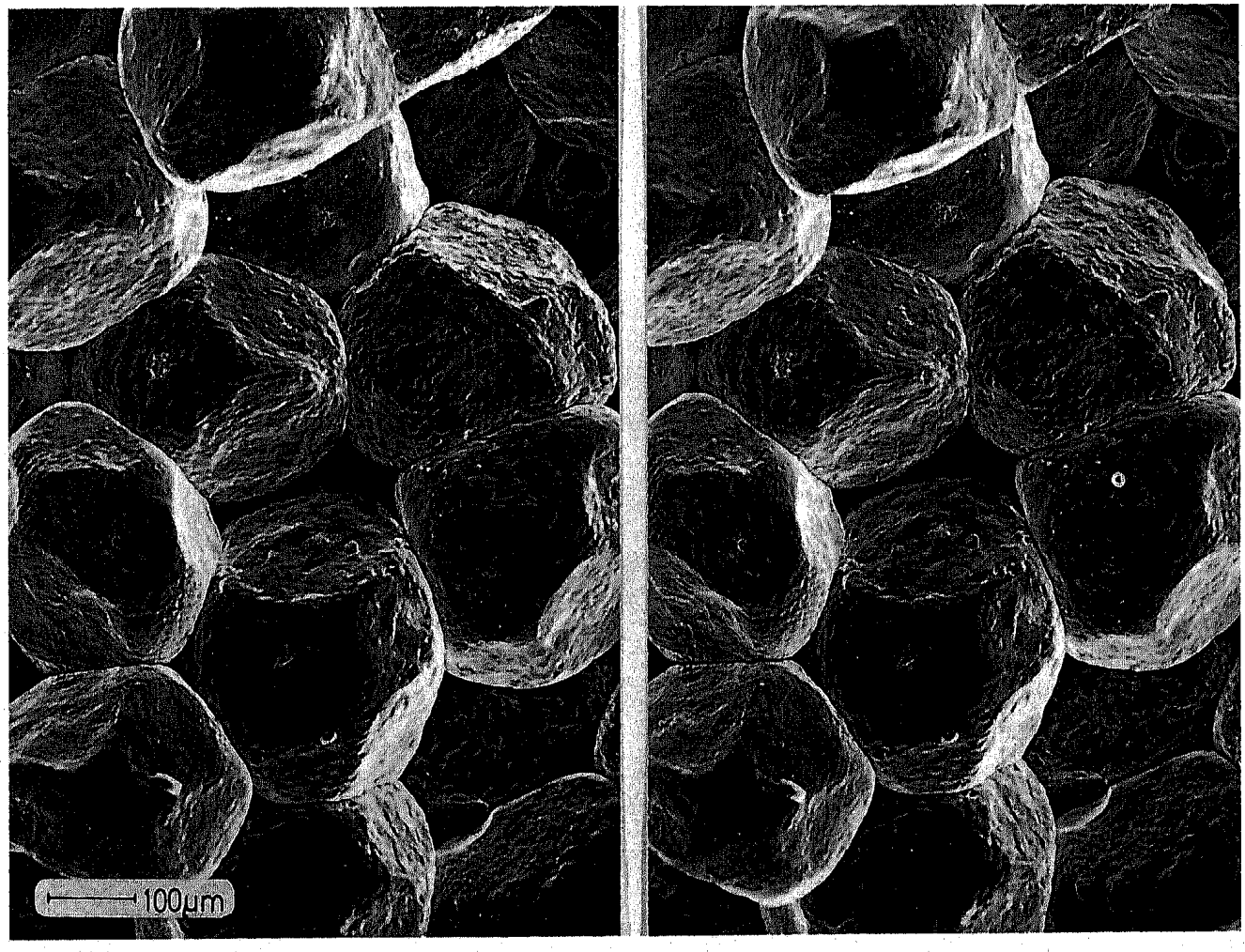

5 Appearance of contact flats in SEM stereo fractograph. Initial contact points marked by sintered necks (presintered 1 h, compacted 1 GNm^{-2}).

for about 10 s. The etchant penetrated into the pores but not between particles in contact, attacking only the free surfaces. The particles were detached from the fracture surface and placed on the sticky side of an adhesive tape for observation under a low-power stereo microscope where the contacts appeared in sharp, bright contrast against the dark background of the etched surfaces. The particles could be observed from all sides by rolling them about with a needle, allowing all facets to be counted. About 50 particles from each specimen were evaluated in this way.

Figure 3 shows a comparison of the average coordination number Z as determined from SEM fractographs and by all-round counting. The latter results are thought to be more reliable because the contact flats are not sufficiently well defined in SEM fractographs for certain detection of the smallest ones. This is believed to be the reason for the large negative deviation of the SEM count for the low-pressure compacts. Figure 4 shows the distribution of coordination numbers among the particles of an uncompacted specimen, and after compaction.

MICROSCOPIC MEASUREMENT OF POROSITY AND CONTACT AREA

The compacts were notched by a saw cut and fractured to reveal the flattened particle contacts. One part was used to make stereo pairs of SEM fractographs (Fig. 5). The other was impregnated with resin and sectioned for quantitative metallographic analysis (Fig. 6).

Point counting with a Zeiss integration eyepiece[22,23] was used to measure the porosity Π, or volume fraction of pores:

$$\Pi = V_V^p = P_p^p \quad . \quad . \quad . \quad . \quad . \quad . \quad . \quad . \quad . \quad . \quad . \quad . \quad . \quad (1)$$

where V_V^p is the volume of pores per unit volume of specimen and P_p^p is the fraction of points (of a test grid superimposed on the microstructure) falling into the pore space (index p).

Derivatives of the principal formulae of quantitative metallography can be found in text books and reviews.[24–26] The error of point counting was estimated by Hilliard's expression[27] for the standard deviation:

$$\sigma^2 = V_V(1-V_V)/P_t. \quad . \quad . \quad . \quad . \quad . \quad . \quad . \quad . \quad . \quad . \quad . \quad . \quad (2)$$

where P_t is the total number of points investigated.

Contact surfaces were measured by lineal analysis, both with the integration eyepiece and with a lineal analyser[28,29] using the principle of specific area measurement:

$$S_V = 2P_L. \quad . \quad . \quad . \quad . \quad . \quad . \quad . \quad . \quad . \quad . \quad . \quad . \quad . \quad . \quad (3)$$

where S_V is the total surface area contained in unit volume of specimen and P_L is the number of intersections between the surface and a test line per unit length of test line.

This can be utilized in two ways.

1. According to Gurland,[30] the 'contiguity' of the metal phase

$$C_m = \frac{2P_L^{mm}}{2P_L^{mm} + P_L^{mp}}. \quad . \quad . \quad . \quad . \quad . \quad . \quad (4)$$

indicates the *fraction* of total particle area which is of metal–metal contact type. (P_L^{mm} is the number, per unit length of test line, of intersections with metal–metal contact surface; P_L^{mp} is the corresponding number of intersections with metal–pore surface.) As long as the particles remain reasonably spherical, their average total particle surface can be expressed as

$$S = 4\pi R^2 \quad . \quad . \quad . \quad . \quad . \quad . \quad . \quad . \quad . \quad . \quad . \quad . \quad . \quad . \quad (5)$$

where R is the volume-weighted mean particle radius. This can be obtained from the size distribution function shown in Fig. 1. If Z is the average number of contacts per particle, we can approximate the average contact area as follows:

$$A \approx \frac{C_m}{Z} \cdot 4\pi R^2 \quad . \quad . \quad . \quad . \quad . \quad . \quad . \quad . \quad . \quad . \quad . \quad . \quad . \quad (6)$$

When particle deformation becomes appreciable, however, this approximation loses its validity.

2. A shape-independent measurement can be based on the quantity

$$S_V^{mm} = 4P_L^{mm} \quad . \quad . \quad . \quad . \quad . \quad . \quad . \quad . \quad . \quad . \quad . \quad . \quad . \quad . \quad (7)$$

which states the *absolute* amount of metal–metal contact area contained in unit volume of specimen. (The factor 4 derives from the factor 2 in eqn. (3) and from the observation that each intersection with a metal–metal contact surface actually belongs to two metal surfaces.) If we change the basis of reference from unit volume of specimen to unit volume of particle phase, we obtain

$$S_{V_m}^{mm} = \frac{4P_L^{mm}}{1-V_V^p} \quad . \quad . \quad . \quad . \quad . \quad . \quad . \quad . \quad . \quad . \quad . \quad . \quad . \quad (8)$$

Introducing the mean particle volume $V = 4\pi R^3/3$, and again using the average number of contacts per particle, Z, we obtain for the average contact area:

$$A = \frac{4P_L^{mm}}{1-V_V^p} \cdot \frac{V}{Z} \quad . \quad . \quad . \quad . \quad . \quad . \quad . \quad . \quad . \quad . \quad . \quad . \quad . \quad (9)$$

The validity of this relation is not affected by changes in particle or contact geometry.

Of course, the average contact area could also be determined from the stereo fractographs by identifying the horizontal (undistorted) dimension of each facet, or by a complete stereometric evaluation of the surface contour. However, the accuracy of such determinations was considered inferior to that of quantitative metallography because the contours of the contact flats are not always sufficiently well defined in the fractographs, and because

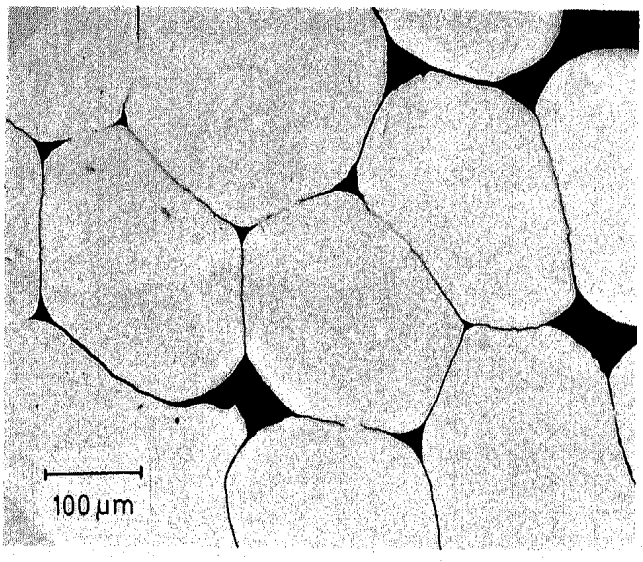

6 Polished section of compact (presintered 1 h, compacted 0·4 GN m^{-2}).

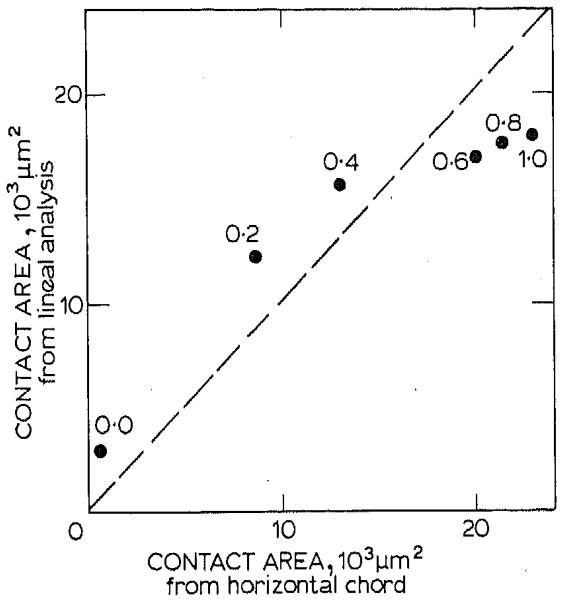

7 Average contact area as determined by quantitative metallography (eqn (9)) compared to values derived from SEM fractographs. Parameter: pressure in GN m^{-2}.

particles at different height levels in the specimen are imaged at slightly different magnification. Most important, however, is the deviation from circularity of the contact contours at higher pressures, which makes the horizontal chord a poor measure of the size of the contact flat.

Figure 7 compares measurements of the average contact area by quantitative metallography (from analyses of about 1200 particle intersects per specimen, evaluated according to eqn. (9)) with estimates based on horizontal diameter measurements in SEM stereo fractographs (assuming the contacts to be circular). Between 130 and 250 contacts were measured in this way for each specimen. For the reasons explained above, greater reliance is placed on the metallographic measurements. The large positive deviation of the SEM measurements at high pressures is attributed to the increasing non-circularity of the contacts combined with a tendency to pick out the longest instead of central chords in measuring the polygonal contacts in SEM fractographs.

MEASUREMENT OF CONTACT ECCENTRICITY (PARTICLE SLIDING)

As mentioned in the introduction, the eccentricity of the final contact flats with respect to their initial points of contact (marked by the sintered necks) can be used to assess the occurrence of non-radial particle motion (sliding). During compaction, the shape of the facet contours changes from circular to polygonal. The centre of a contact facet is taken to be its areal centre of gravity. The distance of this point from the point of initial contact is referred to as the eccentricity of the contact. This was measured by quantitative evaluation of stereo pairs of scanning electron micrographs, cf. Fig. 8. The true length of the vector e is obtained from its components Δx, Δy, and Δz:

$$\mathbf{e} = \sqrt{\Delta x^2 + \Delta y^2 + \Delta z^2} \quad \ldots\ldots\ldots\ldots \quad (10)$$

where the components can be inferred from measurements on the stereo images as described by Krause:[33]

$$\Delta x = \frac{\Delta x_1 + \Delta x_2}{2\cos(\alpha/2)}, \qquad \Delta z = \frac{\Delta x_1 - \Delta x_2}{2\sin(\alpha/2)} \quad \ldots\ldots \quad (11)$$

Here α ($=10°$) is the angle of tilt between the two images, and Δx_1 and Δx_2 are the projected components of **e** as shown in the figure. Distances along the tilt axis y remain undistorted so that

$$\Delta y = \Delta y_1 = \Delta y_2 \quad \ldots\ldots\ldots\ldots \quad (12)$$

The centre of gravity of the contact flat was determined using an apparatus for manual evaluation of micrographs, 'MOP'.[31,32] This is essentially a digitizing board connected to a microprocessor. The stereo images are placed on the board and the contact contours are traced with a cursor. This transmits the coordinates of all contour points to the microprocessor, which then prints out the coordinates of the centre of gravity of the contact flat. The projected position of the initial contact point can be recorded in the same way.

In this manner, some 30 contacts with clearly defined necks were evaluated for each specimen. Figure 9 shows the distribution of the eccentricities in a specimen compacted at 0·6 GN m^{-2}. Its shape, slope, and width are representative of all specimens studied here.

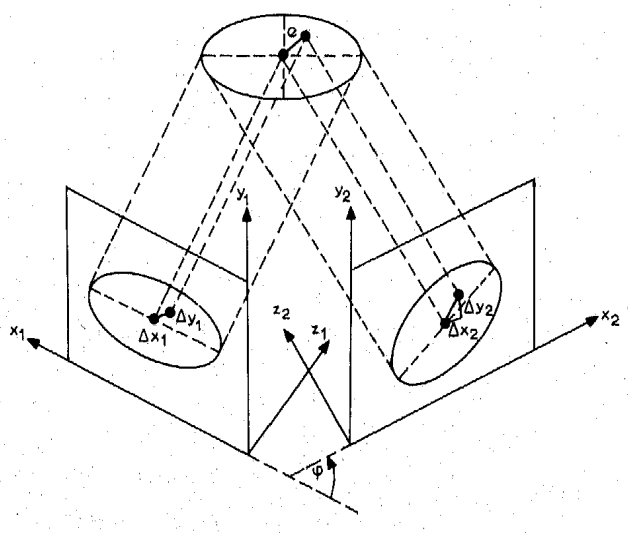

8 Principle of evaluation of stereo fractographs.

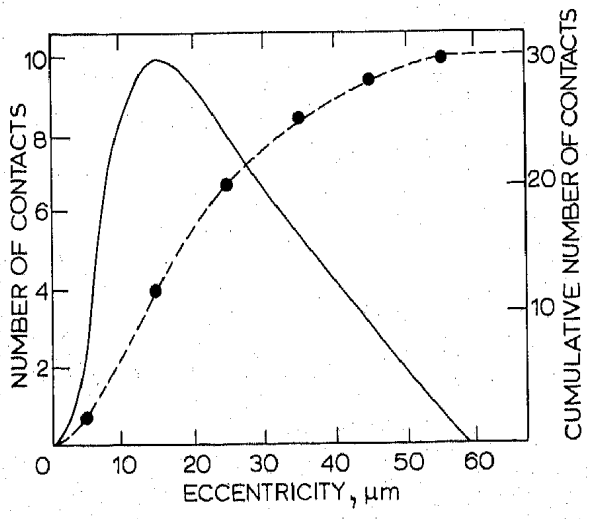

9 Distribution of eccentricity of contact facets to initial contact points after compaction at 0·2 GN m^{-2}.

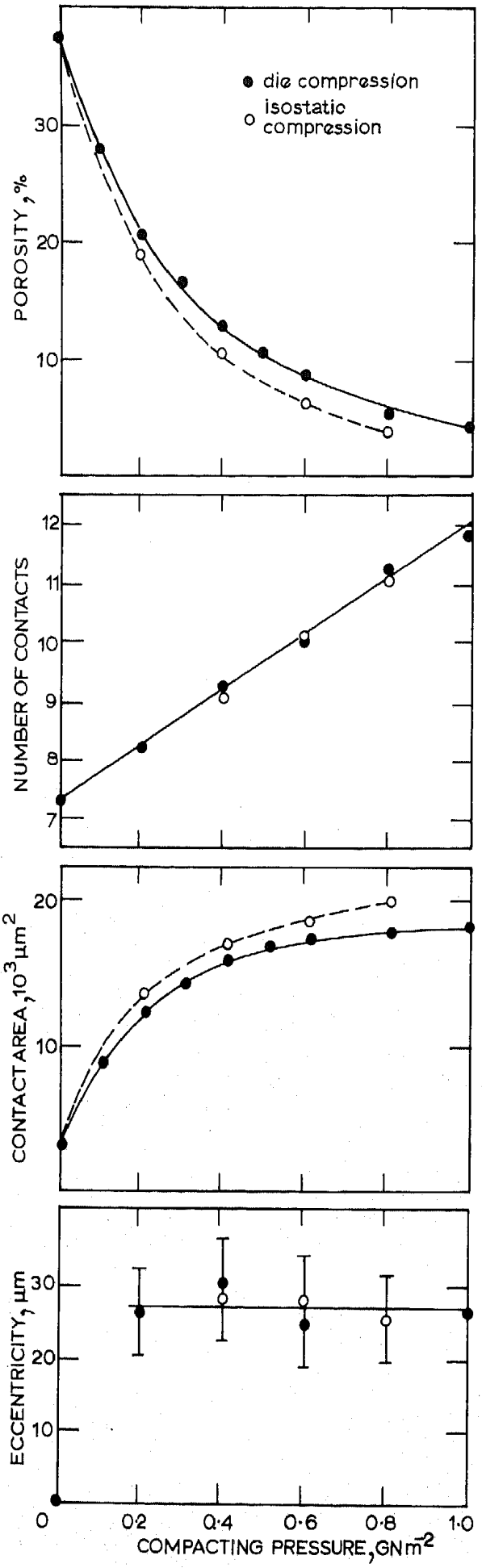

10 **Porosity, coordination number, size, and eccentricity of contact facets vs. pressure for uniaxial and isostatic compacts.**

RESULTS AND DISCUSSION

Figure 10 summarizes the measurements of porosity, coordination number, contact surface, and eccentricity of final vs. initial contact, all as a function of pressure.

The porosities in Fig. 10 are based on the known weights and dimensions of the die-pressed compacts. They were corrected for internal porosity in the particles (about 1 vol.-%) so as to state the net interparticle voidage. For isostatic compacts, porosities were determined by quantitative metallography according to eqn. (1) and calibrated by comparison of quantitative metallographic measurements with weight-and-dimension based values.

The contact surfaces shown in Fig. 10 were determined by quantitative metallography according to eqn. (9). The SEM values reported in Fig. 3 are not included here. Contact surfaces given for the die-pressed compacts are the mean of values for strongly and lightly presintered specimens, since there was no significant difference in contiguity between the

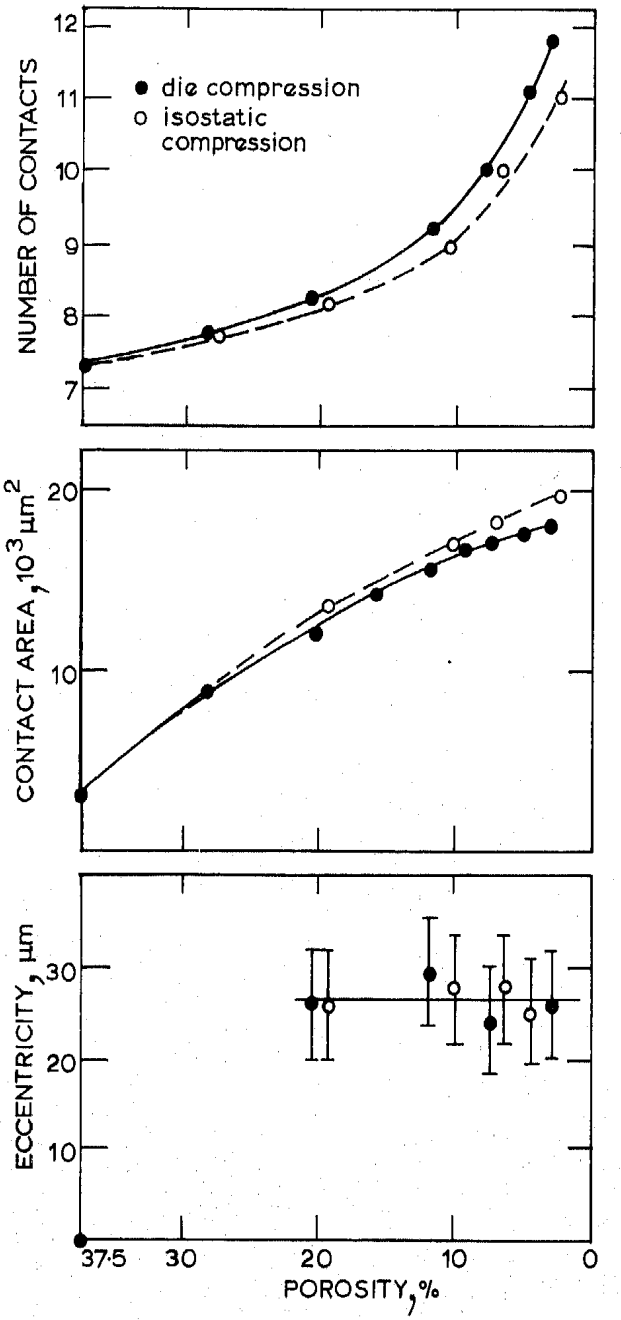

11 **Coordination number, size, and eccentricity of particle contacts vs. porosity for uniaxial and isostatic compacts.**

two types. As it proved difficult to detach individual particles from the strongly presintered compacts, Z-counts were made only on the lightly bonded specimens, and these values were used for the conversion from specific surface to contact surface in all cases. Isostatic experiments were made only with specimens of the lightly bonded type.

It is instructive to consider the various quantities as a function of porosity rather than pressure, as shown in Fig. 11. Before compaction, the powder has a mean coordination number of $Z = 7{\cdot}3$, somewhat below that of a regular bcc or a primitive hexagonal packing ($Z = 8$). Its porosity, at 37·5%, is closer to that of the latter (39·5%); the bcc packing has 32% porosity. However, neither of the regular packings appears really suitable as a model of a powder prior to compaction when the wide variation of void sizes and the difference in mechanical stability is taken into account.

The initial porosity of 37·5% is in good accord with experimental densities of monosize sphere packings observed by other authors,[34–37] which range from 36·3 to 40·9%. Average coordination numbers of disordered sphere packings have been compiled by Ben Aïm and Le Goff[38] and they vary between 6 and 8·5. (In making these comparisons, one should remember that the particles used here were neither strictly monosize nor exactly spherical.)

It is interesting to note (Fig. 4) that the distribution of coordination numbers is initially quite narrow (from 6 to 9 contacts per sphere); as compaction proceeds, it widens rapidly (e.g. $7 < Z < 12$ at about 20% porosity, although the mean coordination has only increased from 7·3 to 8·2) until finally, as the porosity approaches zero, the coordination again becomes more determinate ($10 < Z < 14$). The final coordination is clearly above that for regular close packings of spheres (fcc or hcp with $Z = 12$). The final coordination can again be compared with the results of other authors: Bernal[39,40] has found $Z = 13{\cdot}4$ or 13·6 in fully compacted sphere packings; Coxeter[41] states a theoretical value of 13·6; also it is well known that the truncated octahedron (or tetrakaidekahedron) with 14 faces, forms a good approximation of the average grain or cell shape in polycrystalline metals, ceramics, or in foams.[25,42,43] A final coordination number around 13·5 does not appear implausible for isostatic compacts when considering Fig. 1, although the coordination changes so rapidly at low porosities that extrapolation is very uncertain.

A much safer extrapolation is possible with respect to the mean contact area (cf. Fig. 11). For isostatic compacts, this yields almost exact agreement with the value for a truncated octahedron[44] of the same volume as the mean particle in our powder:

$$V = 8\sqrt{2}\,.\,L^3 = 4\pi R^3/3$$
$$S = 6L^2(1+2\sqrt{3})$$
$$A = S/14 = 20\,174\,\mu m^2$$

where L = edge length and R is 143 μm.

For twelvefold coordination, two polyhedra are possible:

(*a*) the pentagon dodekahedron[45]

$$V = 7{\cdot}663L^3 = 4\pi R^3/3$$
$$S = 20{\cdot}646L^2$$
$$A = S/12 = 23\,297\,\mu m^2$$

(*b*) the rhombic dodekahedron[44]

$$V = 0{\cdot}707d^3 = 4\pi R^3/3$$
$$S = 2{\cdot}121d^2$$
$$A = S/12 = 23\,713\,\mu m^2$$

where d is the face diagonal.

Both of these values are clearly unrealistic in the light of Fig. 10. The conclusion is that the final coordination produced by isostatic compaction seems to be quite well described by the Bernal model, and the final grain shape is better approximated by the truncated octahedron than by either of the dodekahedra which have been used occasionally.

The initial course of the contact-area curves in Figs. 10 and 11 deserves attention as well. If transient restacking occurred as a separate stage before the onset of particle deformation, these curves should start with a horizontal tangent, or at least they should show an inflexion point as deformationless restacking comes to an end. Such an inflexion seems difficult to reconcile with the data points, although measurements at very low porosities were not possible. Since, as shown by the parallelity of the compaction curves in Fig. 2, particle sliding does not seem to have been seriously impeded by the presintering treatment, it looks rather as if both deformation and sliding commenced concurrently (or very nearly so) at the beginning of compaction. Since we are dealing with averages, there will certainly be microregions where deformationless restacking is prevalent, but also others where contact flats are formed at once by plastic deformation.

Figure 11 shows interesting differences between isostatic and axial compaction, in that the contacts formed in die pressing are more numerous and correspondingly smaller than in isostatic compacts. (The measurements pertain to the central part of the die compacts.) The higher coordination number suggests more efficient particle restacking in the early stages of compaction. It is conceivable that particle configurations around voids might be less stable against unidirectional deformation than in hydrostatic compaction. The eccentricity data at the bottom of Fig. 11 have too much scatter to provide direct verification of this conclusion; thus the picture must remain hypothetical. Nevertheless, it does appear plausible that uniaxial compaction could effect better packing before the particles are locked into place around the residual voids.

The friction-induced dissipation of pressure towards the die walls apparently precludes this initially superior packing from making itself felt in better densification throughout a die compact. In keeping with practical experience, Fig. 10 shows that porosity is reduced more efficiently by isostatic pressing, although this mode of compaction seems to depend more on brute plastic deformation, as evidenced by the stronger flattening of the contacts.

The eccentricity of the contact facets with respect to the initial points of contact is plotted at the bottom of Figs. 10 and 11. The obvious conclusion from these plots is that non-radial particle motion (sliding) reaches a saturation level somewhere below 0·2 GN m^{-2}. Additional eccentricity measurements were attempted at 0·1 GN m^{-2} but failed because of the very small contact surfaces developed at that pressure. Thus the data in Figs. 10 and 11 allow only an upper limit to be fixed for the regime of particle sliding. However, there is some indication that sliding does occur up to that limit. Earlier measurements on the same specimens,[46] using a less-developed technique which

allowed only relative determinations, but with a very good statistical basis (130 to 250 contacts per specimen were evaluated) differ from the present ones in that the mean eccentricity at 0·2 GN m^{-2} was only 65% of the shelf value which was fully attained at 0·4 GN m^{-2}. This suggests that particle sliding may in fact be active up to the point where about one-half of the initial porosity has been eliminated.

It must be remembered that the eccentricity of contacts is only a qualitative indicator of the occurrence of particle sliding; quantitative interpretation in terms of its contribution to densification must be difficult. Firstly, a much more detailed model than presently available would be required to translate average eccentricities into reduction of average centre-to-centre distances. It will be remembered that the distribution of eccentricities is quite wide (Fig. 9). Secondly, the motion of all particles not yet in contact at the time of sintering never comes to be reflected in eccentricity. Consequently, relatively large sliding translations could elude detection.

An attempt was made to assess the contribution of particle sliding indirectly by calculating the amount of densification due to the plastic deformation of the particles from the contact-area measurements. Kakar and Chaklader[14] have suggested a model in which the material displaced from the contact zones of spheres in a regular packing is distributed evenly over the remaining free surface. Calculations based on this model yielded a curve of contact surface vs. porosity which almost exactly coincided with that in Fig. 11, leaving no scope at all for a contribution of particle sliding. The conclusion is not that sliding does not contribute to densification, but that the Kakar–Chaklader model overestimates the densification brought about by a given amount of flattening. This is not surprising in the light of experimental and theoretical observations on the flattening of spheres in plastic contact,[2,3] which indicate that most of the material expelled from the contact zone actually stays in its vicinity. This would produce larger contact flats for a given centre-to-centre approach, or conversely, less densification for a given amount of flattening than predicted by the Kakar–Chaklader model. Obviously, a more precise description of the shape change of spheres in plastic contact is needed to advance the treatment of this problem. Work along these lines is in progress.

CONCLUSIONS

1. In the powder studied here, non-radial particle motion (sliding) proceeds well into the plastic stage of densification. It comes to an end at a residual porosity of about 20%.

2. If there is a separate stage of deformationless restacking at the beginning of compaction, it must be very limited. Rather it seems as if deformation and sliding both occur concurrently right from the beginning, although there are probably microregions in which one or the other process occurs alone.

3. There is a continuous increase of particle coordination during compaction (very nearly linear with pressure). The width of the distribution of the individual particles' coordination numbers passes through a maximum at intermediate porosities.

4. The mean size of the particle contacts increases smoothly from the beginning of compaction; towards the end of densification it approaches quite closely the mean size of the faces of a tetrakaidekahedron, or truncated octahedron.

5. The measurements of contact area and coordination number indicate that isostatic compaction involves more deformation at fewer contact points, suggesting that the particle coordination is locked into place earlier than in axial compression.

6. No attempt has been made in this study to test the generality of the observations for different types of powder. Differences in surface roughness, friction properties, surface oxide, and resultant propensity for cold welding as well as yield stress and work hardening of the particle material may well produce changes in the relations observed here.

ACKNOWLEDGEMENTS

The first experiments in this project were made in 1974 by Mr Mats Strömgren and Mr Ted Böklin, then undergraduates at Chalmers University of Technology. Continuation and conclusion of the work at Montanuniversität Leoben was made possible by a grant from the Austrian Science Research Council.

REFERENCES

1. K. ZANDER: *Powder Metall. Int.*, 1970, **2**, 129.
2. P. WELLNER, G. H. GESSINGER, and H. E. EXNER: *Z. Metallkd.*, 1974, **65**, 602.
3. B. O. SUNDSTRÖM and H. F. FISCHMEISTER: *Powder Metall. Int.*, 1973, **5**, 171.
4. N. HELLIWELL and P. J. JAMES: *ibid.*, 1975, **7**, 25.
5. P. J. JAMES: *Powder Metall.*, 1977, **20**, 21.
6. P. J. JAMES: *ibid.*, 1977, **20**, 199.
7. G. BOCKSTIEGEL and J. HEWING: *Arch. Eisenhüttenwes.*, 1965, **36**, 751.
8. P. J. JAMES: *Powder Metall. Int.*, 1972, **4**, pp. 82, 145, and 193.
9. M. J. DONACHIE and M. F. BURR: *J. Met.*, 1963, **15**, 849.
10. R. W. HECKEL: *Trans. AIME*, 1961, **221**, 671 and 1001.
11. A. DUFFIELD and P. GROOTENHUIS: Symp. Powder Met., p. 96. **1954**: London (Iron Steel Inst.).
12. E. TURBA: *Proc. Br. Ceram. Soc.*, 1965, **3**, 101.
13. G. BOCKSTIEGEL: 'Modern developments in powder metallurgy', (ed. H. H. Hausner), vol. I, p. 155. **1966**: New York (Plenum Press).
14. A. K. KAKAR and A. C. D. CHAKLADER: *J. Appl. Phys.*, 1967, **38**, 3223.
15. M. C. KOSTELNIK, F. H. KLUDT, and J. K. BEDDOW: *Int. J. Powder Metall.*, 1968, **4**(4), 19.
16. A. L. STUIJTS and G. J. OUDEMANS: *Proc. Br. Ceram. Soc.*, 1965, **3**, 81.
17. R. L. HEWITT, W. WALLACE, and M. C. de MALHERBE: *Powder Metall.*, 1974, **17**, 1.
18. M. STRÖMGREN, H. ÅSTRÖM, and K. E. EASTERLING: *ibid.*, 1973, **16**, 155.
19. H. FISCHMEISTER, B. ARÉN, and K. E. EASTERLING: *ibid.*, 1971, **14**, 144.
20. B. ARÉN, L. OLSSON, and H. FISCHMEISTER: *Powder Metall. Int.*, 1972, **4**(3), 1.
21. J. WALLNER: *Berg Hütten-mann. Monatsh.*, 1964, **109**, 107.
22. A. HENNING: *ZEISS Werkzeitschr.*, 1958, **6**, 78.

23. J. GAHM: *ZEISS Mitt.*, 1971, **5**, 249.
24. R. T. DeHOFF and F. N. RHINES: 'Quantitative microscopy'. **1968:** New York (McGraw-Hill).
25. E. E. UNDERWOOD: 'Quantitative stereology'. **1970:** Reading, Mass. (Addison-Wesley).
26. H. FISCHMEISTER: *Powder Metall. Int.*, 1975, **7**, 178.
27. J. E. HILLIARD and J. W. CAHN: *Trans. AIME*, 1961, **221**, 344.
28. H. FISCHMEISTER: *Z. prakt. Metallogr.*, 1965, **2**, 251.
29. H. FISCHMEISTER: Symp. Métall. des Poudres, Paris, 1964, p. 115 (Edition Métaux).
30. J. GURLAND: *Trans. AIME*, 1958, **212**, 452.
31. G. HILLJE and G. REDMANN: *Prakt. Metallogr.*, 1976, **7**, 629.
32. 'MOP information brochure'. **1977:** München (KONTRON Messgeräte).
33. H. KRAUSE: *Freiberger Forsch.*, 1970, **A485**, 49.
34. W. A. GRAY: 'Packing of solid particles'. **1968:** London (Chapman and Hall).
35. A. E. R. WESTMAN and H. R. HUGILL: *J. Amer. Ceram. Soc.*, 1930, **13**, 767.
36. G. D. SCOTT: *Nature*, 1960, **188**, 908.
37. J. C. MACRAE and W. A. GRAY: *Br. J. Appl. Phys.*, 1960, **12**, 164.
38. R. BEN AÏM and P. LE GOFF: *Powder Technol.*, 1968, **2**, 1.
39. J. D. BERNAL: *Nature*, 1959, **183**, 141.
40. J. D. BERNAL: 'Liquids: structure, properties, solid interactions' (ed. T. J. Hughel), p. 26. **1965:** Amsterdam (Elsevier).
41. H. S. M. COXETER: *Illinois J. Math.*, 1958, **2**, 746.
42. C. S. SMITH: *Trans. AIME*, 1948, **175**, 15.
43. R. L. COBLE: *J. Appl. Phys.*, 1961, **32**, 787.
44. E. E. UNDERWOOD: Ref. 24, p. 91.
45. 'Handbook of chemistry and physics', 44th Edn., p. 346. **1962:** Cleveland, Ohio (Chemical Rubber Publ. Co.).
46. T. BÖKLIN and L. OLSSON: unpublished results, Chalmers Univ. of Technol., 1974.